PCCP

Accepted Manuscript




ROYAL SOCIETY OF CHEMISTRY

www.rsc.org/pccp

PCCP

RSCPublishing

ARTICLE

# Mechanism of N-Ag Bonding Determined Tunability of Surface-Enhanced Raman Scattering of Pyridine on MAg (M=Cu, Ag, Au) Diatomic Clusters

Cite this: DOI: 10.1039/xoxxoooooox

Received ooth January 2012,
Accepted ooth January 2012

DOI: 10.1039/xoxxoooooox

www.rsc.org/

Lei Chen,[a,b] Yang Gao,[b] Haoran Xu,[a] Zhigang Wang,*[b,c] Zhengqiang Li,*[a] and Rui-Qin Zhang,*[d,e]

Binary coinage metal clusters can show significantly different enhancement in surface-enhanced Raman scattering (SERS) from that of pure element clusters, owing to their tunable surface plasmon resonance energies affected by the composition and atomic ordering. Yet, the tunability by composition requires a deep understanding in order to further optimize the SERS-based detection technique. Here, to fill this deficiency, we conducted detailed analyses of the SERS of pyridine adsorbed through N-Ag bonding on the homonuclear diatomic metal cluster $Ag_2$ and heteronuclear diatomic metal clusters of AuAg and CuAg, as well as the involved charge transfer under an intracluster excitation, based on calculations using time-dependent density functional theory with a short-time approximation for the Raman cross-section. We find that although the SERS enhancements for all complexes can reach the order of $10^3$-$10^4$, the corresponding wavelengths used for SERS excitation are significantly different. Our molecular orbital analysis reveals that the complexes based on heteronuclear metal clusters can produce varied electronic transitions owing to the polarization between different metal atoms, which tune the SERS enhancements with altered optical properties. Our analyses are expected to provide a theoretical basis for exploring the multi-composition SERS substrates applicable for single molecular detection, nanostructure characterization, and biological molecular identification.

## 1 Introduction

Since the discovery of surface-enhanced Raman scattering (SERS) in the 1970s,[1] the relationship between SERS substrates and SERS enhancements has become the key issue for researchers in the SERS field. With the development of nanotechnology, there is a growing interest in using mixed-metal materials as the substrate. In the past decade, multi-composition SERS substrates based on coinage metals has been widely used as a powerful analytical tool in many fields, such as surface analysis, biotechnology, single-molecule detection, etc.[2-5] It is generally believed that enormous SERS signal enhancement arises mainly from two mechanisms:[6-9] (a) enhanced local electromagnetic fields due to excitations in the metal cluster (the EM mechanism), and (b) resonance enhancements caused by charge transfer between the molecule and metal cluster due to excitations (the CT mechanism). Many research findings indicate that, superior to pure coinage metal clusters, the mixed-metal clusters can tune their own and the molecule-metal's optical properties by varying the composition so as to tune SERS enhancements.[2,4,5,10]The presence of the heteronuclear metal atoms changes the electronic properties of clusters, as well as their Fermi levels, band gaps, and electronic orbitals.[11,12] The complicated and changeable structures of the mixed-metal clusters allow optimization of the structure to fulfil the requirements of SERS detection.

In fact, intensive studies have been conducted to achieve optimal matching between SERS substrates and excitation light in order to maximize the SERS signal, by introducing another metal into silver substrates.[2,3,13] The hybrid metallic cluster exhibits a tunable plasmon resonance frequency and thus makes it easier to obtain single-molecule vibrational spectroscopy. Most SERS experiments have been based on visible-light excitation, at such as 532, 514, and 488 nm, using blue and green lasers. According to the literature, single-molecule detection can be achieved with excitation light in this range.[14-19] Nie and colleagues achieved single-molecule SERS (SM-SERS) signals of rhodamine 6G and inaugurated the era of single-molecule detection with SERS technology.[17] Xu et al. detected SM-SERS signals of hemoglobin.[19] Their experiments were all based on silver nanoparticles with excitation wavelength of 514 nm. In 2013, Partha measured the SM-SERS spectroscopy of rhodamine 6G on Au/Ag bimetallic clusters with excitation wavelength of 532 nm.[4] This was the first SM-SERS detection on bimetallic clusters and at an incident wavelength of 532 nm. Clearly, the excitation wavelength is closely related to the composition of clusters for SM-SERS detection.

First-principles approaches are powerful tools to understand the SERS mechanism and have been widely used to describe the SERS enhancement of molecules adsorbed onto small metal clusters.[20-24] Wu and colleagues simulated pyridine adsorbed onto small coinage metal clusters by employing the Hybrid Density Function Theory (DFT) method, and the obtained bonding properties and Raman spectra show agreement with experimental data.[20,25] Jensen et al. developed a Time-Dependent Density Functional Theory (TDDFT) method implemented in the Amsterdam Density Functional (ADF) program by considering the finite lifetime of the electronic excited states in linear-response theory.[26] They presented a detailed analysis of the enhanced Raman scattering of the pyridine-$Ag_{20}$ model system with the developed TDDFT method and their results show different contributions to the SERS enhancements from previous studies, including CT enhancements ($10^3$) and EM enhancements ($10^5$).[21-23] Birke and colleagues calculated the resonance Raman spectra of a $Ag_{10}$-pyridine vertex complex using the TDDFT method.[27] And now the TDDFT method is widely accepted and applied in SERS simulations.

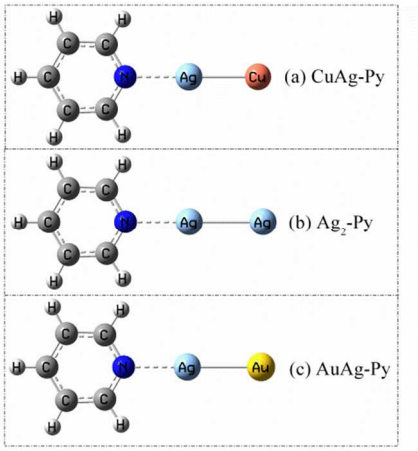


Figure. 1 Optimized geometries for the MAg-Py (M=Cu, Ag, Au) at the level of BP86/TZP.

Since the SERS signal of pyridine was first detected in 1974, this small molecule has become one of the most commonly used adsorbates in theoretical and experimental investigations. Silver is recognized as one of the best materials for SERS enhancement and is thus adopted in this study to form coinage diatomic clusters with Au and Cu atoms as SERS substrates. Silver material has been testified to be the best substrate for SERS enhancement. As we all know, all the target molecules are almost adsorbed on silver substrate via N-Ag bonding in experiments. For silver clusters, the linear combination of s orbital allows the Ag atoms to provide symmetry-adapted s orbital to receive the lone pair of electrons of the N atom. And numerous studies show that the most favorable bonding between the pyridine and silver metal atomic dimer is through the HOMO of pyridine interacting with the LUMO of metal clusters along the M-M bond axis direction. Studies in this work include the homonuclear cluster $Ag_2$ and heteronuclear clusters of AgAu and AgCu, all possessing stable closed-shell configurations.[28] Absorption and SERS spectra of pyridine interacting with these clusters were calculated in order to show the tunability mechanism of SERS enhancement caused by the varied composition of the metal clusters. As shown in Figure 1, the pyridine molecule is adsorbed onto metal clusters via the N-Ag bonding. The geometries shown in Figure 1 are all optimized at the BP86/TZP level, and all of them are stable. However, for pyridine-metal complexes, the composition difference of metal clusters can cause the change in electronic absorption spectra, resulting in different SERS enhancement of target molecules. Our previous DFT study revealed that the chemical enhancements and binding properties of pyridine on mixed-metal clusters strongly depend on binding sites.[11] In this article, an intensive study of the tunability mechanism of SERS enhancements is presented based on calculations by employing the recently developed TDDFT method.

## 2 Computational methods

The conventional DFT method is only suitable for computing chemical enhancements in SERS.[12,29] In contrast, the recently developed TDDFT[26] method implemented in the ADF program package[30] can simulate both chemical and EM enhancement for pyridine adsorbed onto metal clusters.[21,22,27] The new method is based on a short-time approximation to the Raman cross-section. All calculations in this study have been done by employing the ADF program package. The Becke-Perdew (BP86) XC-potential[31] and a triple-ξ polarized Slater type (TZP) basis set from the ADF basis set library have been used. A full electron basis set has been used for N, C, and H. Whereas the 1s-2p core has been frozen for Cu and 1s-3d core for Ag, and 1s-4f core for Au, respectively.[23,32,33] Scalar relativistic effects have been accounted for by means of the zeroth-order regular approximation (ZORA).[34] The vibrational frequencies calculated with the BP86 functional are close to experimental results even without the use of scaling factors.[35] Vibrational frequency analysis is performed after obtaining the optimized geometries and all vibrational frequencies obtained for the electronic ground states are real.

Absolute Raman intensities are presented as the differential Raman scattering cross-section (DRSC) in terms of the derivative of the polarizability. For Stokes scattering with an experimental setup of a 90° scattering angle and perpendicular plan-polarized light, the cross-section is given as follows[36]

$$I_{Raman} = \left(\frac{d\sigma}{d\Omega}\right)_i = \frac{(2\pi)^4}{45}\frac{h}{8\pi^2 c\omega_i}\frac{(\omega_0-\omega_i)^4}{1-\exp(-hc\omega_i/k_BT)}\left[45\left(\frac{d\alpha}{dQ_i}\right)^2+7\left(\frac{d\gamma}{dQ_i}\right)^2\right] \quad (1)$$

Here, $\omega_0$ and $\omega_i$ are the frequencies of the incident light and the ith vibrational mode, respectively, and h, c, $k_B$, and T are the Planck constant, light speed, Boltzmann constant, and Kelvin temperature, respectively; $d\alpha/dQ_i$ and $d\gamma/dQ_i$ are the derivatives of the isotropic and anisotropic polarizability of the ith vibrational mode, respectively. The electronic polarizability of both on- and off-resonance Raman scattering is calculated by including a finite lifetime (using a damping parameter $\Gamma \approx$ 0.004 a.u.) of the electronic excited states in the TDDFT polarization calculations.[26]

## 3 Results and Discussion

### 3.1 UV-visible absorption spectra

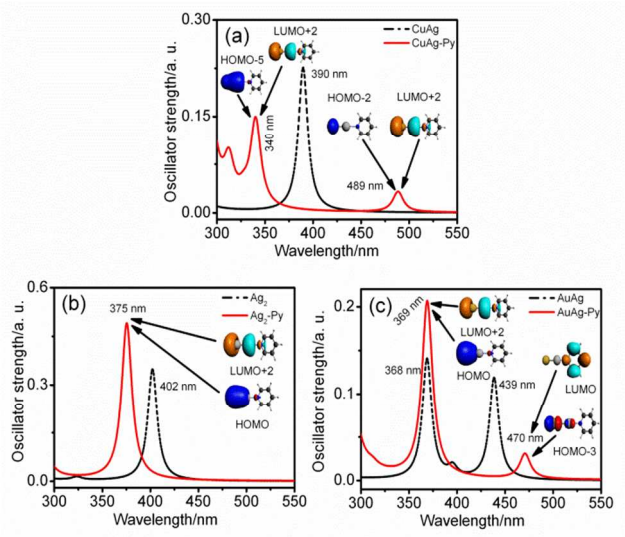


Figure. 2 UV-Visible absorption spectra of CuAg-py, $Ag_2$-py, and AuAg-Py complexes as well as their corresponding bare metal clusters. Black lines denote the results of bare metal clusters of CuAg, $Ag_2$, and AuAg; red lines denote the results of bare metal clusters of CuAg-py, $Ag_2$-py, and AuAg-Py complexes. Absorption coefficients are given as the oscillator strength in a.u. and wavelength in nm. Spectra have been broadened by a Lorentzian function with a width of 0.1 eV.

Based on the optimized structures, absorption spectra in the range from 300 to 550 nm are obtained by TDDFT calculations. Figure 2 shows the specific changes in the absorption spectra of $Ag_2$-Py, AuAg-Py, and CuAg-Py complexes as well as the corresponding bare metal clusters. For $Ag_2$ and AgAu clusters, the absorption peaks of our calculations for low singlet states ($S_0 \rightarrow S_1$) are calculated to be 3.08 and 2.83 eV, respectively, which correspond to absorption peaks at 402 nm for $Ag_2$ and 439 nm for AgAu. Relating to the above, the experimental excitation energies are 2.8 eV for $Ag_2$ and 2.73 eV for AgAu clusters,[28] respectively. For the CuAg cluster, the maximum absorption peak is calculated to be 3.18 eV (390 nm), in good agreement with experimental value 3.20 eV.[28] We can see that the absorption spectra change considerably for each complex, and the absorption peaks are mainly located in the range 340 to 500 nm. To further understand the electronic behavior of various adsorption systems, we analyzed the electron radiation transitions, the detailed data of which are presented in Table 1. The absorption spectra and electronic transitions indicate that there are two electronic transition mechanisms contributing to absorption peaks: a) charge-transfer transitions from the metal cluster to the molecule, which contributes to the CT enhancement in SERS; b) electronic transitions limited to the metal cluster (an analogue to surface plasmon resonance in large nanoparticles), which contributes to IE enhancement (enhancement for intracluster excitation) in SERS.[23,29,32,33] It is clear that the original peaks of the clusters disappear in the absorption spectra after the combination of pyridine on metal clusters, and new peaks appear at other frequencies. The corresponding electronic transitions of absorption peaks of the bare metal clusters CuAg, $Ag_2$, and AuAg are given in Fig. S1†, and the peaks show significant differences in location and intensity between the homonuclear cluster $Ag_2$ and heteronuclear clusters AuAg and CuAg.

Figure 2(a) shows the calculated absorption spectra of the CuAg cluster and CuAg-Py complex. For the CuAg cluster, the strongest peak is located at 390 nm, which could be ascribed to the electronic transitions of HOMO-5 → LUMO, and Fig. S1(a)† indicates that this peak is mainly caused by electronic transitions from the Ag atom to the whole cluster as a result of polarization between the Cu and Ag atoms. After the adsorption of pyridine onto CuAg, the peak at 390 nm disappears and two new peaks arise, at 340 and 489 nm. The peak at 340 nm is ascribed to electronic transitions of HOMO-5→LUMO+2, and electronic transitions of this peak derive from the peak at 390 nm of the CuAg cluster. The peak at 489 nm comes from electronic transitions of HOMO-2 → LUMO+2, and it is interesting that these electronic transitions cause charge diffusion from the Cu atom, which spreads evenly to the whole cluster. We note that the corresponding electronic transitions of the peaks at both 340 and 489 nm are all localized on the metal cluster (an analogue to surface plasmon excitation in large nanoparticles). Therefore, SERS based on IE enhancement can be achieved using these two excitation wavelengths. Although the peak intensity at 489 nm is much weaker than that at 340 nm (the oscillating strength is 0.028 for 480 nm and 0.135 for 340 nm), the SERS experiment is more feasible if using the former because it is close to the most commonly used 488 nm excitation wavelength in the visible region, while the peak at 340 nm lies in the ultraviolet region and excitation wavelengths in this region are seldom used in SERS experiments.

Table. 1 The oscillator strength, the corresponding wavelength (nm), and the orbital transitions in MAg-Py (M=Cu, Ag, Au) complexes and the corresponding bare metal clusters.

| Geometry | Wavelength (nm) | Oscillating strength | Orbital transition |
|---|---|---|---|
| CuAg | 390 | 0.225 | HOMO-5→LUMO |
| CuAg-Py | 340 | 0.135 | HOMO-5→LUMO+2 |
| | 489 | 0.028 | HOMO-2→LUMO+2 |
| $Ag_2$ | 402 | 0.348 | HOMO→LUMO |
| $Ag_2$-Py | 375 | 0.487 | HOMO→LUMO+2 |
| AuAg | 368 | 0.139 | HOMO-3→LUMO |
| | 439 | 0.118 | HOMO→LUMO |
| AuAg-Py | 369 | 0.202 | HOMO→LUMO+2 |
| | 470 | 0.029 | HOMO-3→LUMO |

Figure 2(b) presents the absorption spectra of the homonuclear cluster $Ag_2$ and corresponding complex $Ag_2$-Py, with one peak each, at 402 nm for $Ag_2$ and at 375 nm for $Ag_2$-Py. These results are consistent with previous reports.[32] For the $Ag_2$ cluster, the strongest peak at 402 nm could be ascribed to electronic transitions from HOMO to LOMO, as shown in Fig. S1(b)†, and the two Ag atoms make equal contributions to this peak. Compared to the isolated cluster, the absorption maximum of the $Ag_2$-Py complex blue-shifts 27 nm and its oscillator strength increases to 0.487 from the 0.348 of $Ag_2$. Figure 2(a) indicates that the peak at 375 nm comes from

electronic transitions of HOMO → LUMO+2, and the corresponding transition is mainly located on the $Ag_2$ cluster. Thus, SERS based on IE enhancement can be achieved with an excitation wavelength of 375 nm.

The absorption spectra of the AuAg cluster and AuAg-Py complex are shown in Figure 2(c). For AuAg, there are two strong peaks, located at 368 and 439 nm, and the corresponding electronic transitions are from HOMO-3 to LUMO and from HOMO to LUMO, respectively. Fig. S1(c)† indicates that contributions from the Au and Ag atoms are different on account of polarization between these two atoms. For the AuAg-Py complex, the strongest peak appears at 369 nm with a red-shift of 1 $cm^{-1}$ from the peak of AuAg at 368 nm, and its oscillator strength increases significantly. After the adsorption with pyridine, the peak of AuAg at 368 nm turns into 369 nm in the AuAg-Py complex, and the corresponding electronic transitions are from HOMO to LUMO+2. However, the peak at 439 nm disappears and a new peak emerges at 470 nm with an oscillator strength of 0.029 in the AuAg-Py complex, and the corresponding electronic transitions are from metal to pyridine (charge transfer transitions) as shown in Figure 2(c). So IE-enhanced SERS can be achieved with an excitation wavelength of 369 nm and CT-enhanced SERS can be achieved with an excitation wavelength of 470 nm. It is more feasible for the SERS experiment to detect the peak at 470 nm than at 369 nm because it is close to the most commonly used 488 nm excitation in the visible region.

In the absorption spectra of the CuAg-py, $Ag_2$-py, and AuAg-Py complexes in Figure 2, there are many obvious differences despite pyridine being adsorbed onto the silver atoms in all these cases. For the CuAg-py and AuAg-Py complexes, new absorption peaks appear near the blue light region, which can be used to excite SERS in experiments. It is evident that the tunable electronic properties of pyridine-metal complexes are achieved by varying the composition of the metal cluster.

### 3.2 Enhanced Raman Scattering

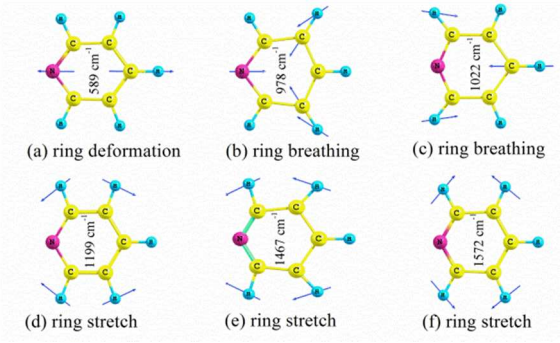


Figure. 3 Frequencies of enhanced vibrational modes for pyridine molecules.

Six vibrational modes of the pyridine which are commonly known are given in Figure 3 for latter comparison. Those modes are expected to be influenced more by the interaction with metal clusters because they involve vibrational motion of the N atom along the N-Ag bond or consist mainly of C-C stretching vibrations with the carbon next to nitrogen vibrating toward the metal cluster.[37]

**Static enhancement:** The interactions between pyridine and the metal clusters result in changes in the polarizability, which will affect the pyridine's Raman spectra, as shown in the wavenumber range between 400 and 1800 cm-1 in Figure 4.

We note that for pyridine alone, the static differential Raman cross-section (DRSC) is of the order of $10^{-31}$ $cm^2$/sr, as shown in Figure 4(a). The intensities are enhanced by a factor of about 40 for the CuAg-Py, 2 for the $Ag_2$-Py, and 4 for the AuAg-Py complexes. The static Raman enhancement due to composition variations of metal clusters is therefore of the order of 10-$10^2$. Ring breathing modes at 978, 1022 $cm^{-1}$ and ring stretch mode at 1573 $cm^{-1}$ dominate the static Raman spectrum of pyridine, and these three modes and other weaker modes are more intense in the calculated spectra of different complexes. Shifts in the vibrational frequencies are observed for all complexes. The largest shifts observed are by about 20-30 $cm^{-1}$ for the modes at 598, 978, and 1573 $cm^{-1}$ because these modes are more sensitive to interaction between pyridine and metal clusters,[21,37] while other modes at 1022, 1199 and, 1467 $cm^{-1}$ are found to have shifts smaller by only several wavenumbers.

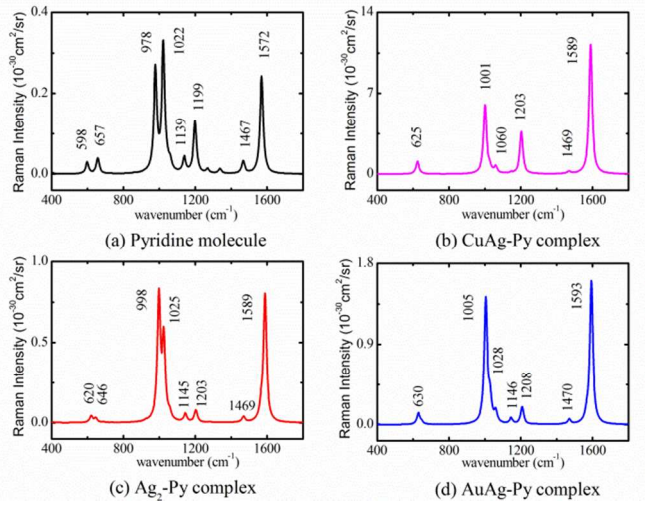


Figure. 4 Calculated static Raman spectra of (a) pyridine, (b) CuAg-Py, (c) $Ag_2$-Py, and (d) AuAg-Py complexes based on static polarizability derivatives. Differential cross-section is measured in the unit of $10^{-30}$ $cm^2$/sr and wavenumber in $cm^{-1}$. The spectra have been broadened by a Lorentzian function to a width of 20 $cm^{-1}$.

**IE enhancement and CT enhancement:** It is generally believed that enormous SERS signal enhancement arises mainly from two mechanisms:6-9 (a) local electromagnetic fields due to excitations in the metal cluster, and (b) resonance caused by charge-transfer excitations between the molecule and metal clusters. However, our calculation indicates that the dominant factor in SERS enhancement is closely related to the composition of clusters and excitation wavelength.

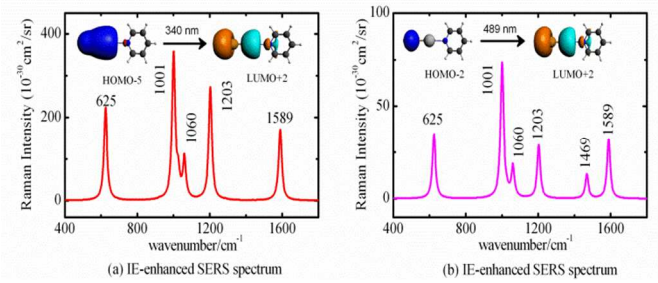


Figure. 5 Calculated SERS spectra of the CuAg-Py complex: (a) for the IE-enhanced SERS spectrum at an incident light wavelength of 340 nm, and (b) for the IE-enhanced SERS spectrum at an incident light wavelength of 489 nm.

The absorption spectra of CuAg-Py, $Ag_2$-Py, and AuAg-Py change significantly in the range 300 to 550 nm, and excitation lights within this range are often used in SERS experiments, especially in SM-SERS detection.[14-19] Next, the IE and the CT mechanisms in SERS enhancement are presented by using excitation wavelengths in the range 300 to 550 nm. The SERS spectra based on different resonance excitations are listed in Figures 5-7 for pyridine adsorbed on CuAg, $Ag_2$, and AuAg clusters.

There are two resonance absorption peaks in the absorption spectra of CuAg-Py, at 340 and 489 nm, whose corresponding SERS spectra, denoted SERS (340 nm) and SERS (489 nm), are presented in Figure 5. The intensities of both Raman spectra are all in the order of $10^{-28}$ cm$^2$/sr, presenting an enhancement of the order of $10^3$ compared to the $10^{-31}$ cm$^2$/sr of pyridine.[21] Molecular orbital analysis results indicate that SERS (340 nm) and SERS (489 nm) are mainly caused by excitations of electronic transitions confined to metal clusters and a small number of charge transfers to the molecule, showing an IE mechanism. A comparison of these two spectra reveals the main changes in the intensities with quite similar features except the absence of the ring stretch mode at 1589 cm$^{-1}$ in the SERS (340 nm) spectrum. Among the six selected modes, that at 1001 cm$^{-1}$ shows the largest DRSC. However, the intensity of SERS (340 nm) is four times that of SERS (489 nm) since the oscillating strength of electronic transitions from HOMO-5 to LUMO+2 is about four times greater than that from HOMO-2 to LUMO+2. Because the 489 nm excitation light is in the visible region and is closer to the most commonly used 488 nm laser than the 340 nm excitation light in the ultraviolet region in experiments, the SERS (489 nm) is more likely to be detected in SERS experiments. In addition, it is very interesting that the electronic transitions responsible for SERS (340 nm) are mainly from the Ag atom, while for SERS (489 nm), the electronic transitions are all from the Cu atom. This is a unique feature of heterogeneous binary clusters.

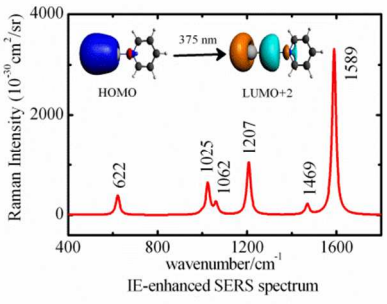


Figure. 6 The IE-enhanced SERS spectrum of an $Ag_2$-Py complex at an incident wavelength of 375 nm.

Significantly different from the results of CuAg-Py, there is only one absorption peak at 375 nm in the absorption spectrum of $Ag_2$-Py complex, whose SERS spectrum, denoted SERS (375 nm), is shown in Figure 6. The intensity of the order of $10^{-26}$ cm$^2$/sr corresponds to an enhancement of the order of $10^4$ from the $10^{-31}$ cm$^2$/sr of pyridine. Molecular orbital analysis results in Figure 6 indicate that the SERS at 375 nm is mainly caused by electronic transitions confined to the $Ag_2$ cluster and small charge transfers to the molecule, showing an IE enhancement mechanism. The ring stretch mode at 1589 cm$^{-1}$ shows the largest enhancement and the result is consistent with previous literature.[32]

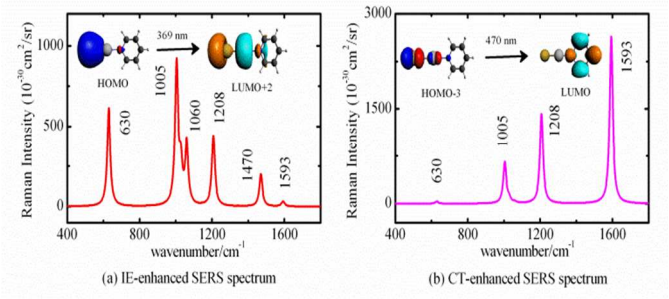


Figure. 7 SERS spectra of the AuAg-Py complex: (a) an IE-enhanced spectrum at an incident wavelength of 369 nm, and (b) a CT-enhanced spectrum at an incident wavelength of 470 nm.

The absorption spectrum of AuAg-Py shows two resonance peaks, at 369 nm in the ultraviolet region and 470 nm in the visible region, and their corresponding SERS spectra, denoted SERS (369 nm) and SERS (470 nm), are presented in Figure 7. The intensities of SERS (369 nm) and SERS (470 nm) are both in the order of $10^{-27}$ cm$^2$/sr, representing an enhancement of the order of $10^4$ from the $10^{-31}$ cm$^2$/sr of pyridine. Molecular orbital analysis results in Figure 7 indicate that SERS (369 nm) is mainly caused by electronic transitions confined to the metal cluster, showing an IE enhancement, while SERS (470 nm) is due to excitation by charge-transfer from the metal cluster to pyridine, indicating a CT enhancement. In addition, it is a unique phenomenon of heterogeneous binary clusters that the electronic transitions which contribute to SERS (369 nm) are all from the Au atom, while for SERS (470 nm), the electronic transitions are mainly from the Au atom. A comparison of these two spectra revealed very different shapes and intensities. In the SERS (369 nm) spectrum, the ring breathing mode at 1005 cm$^{-1}$

shows the largest DRSC, followed by the ring deformation mode at 630 $cm^{-1}$, while the ring stretch mode at 1593 $cm^{-1}$ is almost invisible. However, in the SERS (470 nm) spectrum, the ring stretch mode at 1593 $cm^{-1}$ shows the largest DRSC, followed by the ring stretch mode at 1208 $cm^{-1}$, and the modes at 1470 and 630 $cm^{-1}$ are almost invisible. In addition, the enhancement of SERS (470 nm) is three times that of the SERS at 369 nm. Although the oscillator strength of electronic transitions from HOMO to LUMO+2 (0.202, corresponding absorption peak at 369 nm) is about six times that from HOMO-3 to LUMO (0.029, corresponding absorption peak at 470 nm), the modes at 1593 and 1208 $cm^{-1}$ both involve motions of the atoms at which the LUMO orbital is localized, explaining why the enhancements of SERS (470 nm) are more intense than those of SERS (369 nm). Moreover, in contrast to the 369 nm excitation light in the ultraviolet region, the 470 nm excitation light lies in the visible region and is close to the 488 nm laser most commonly used in experiments. Thus, SERS (470 nm) is more likely to be detected in SERS experiments.

## Conclusions

In a previous study based on the density functional theory approach, we found that the chemical enhancement of SERS is closely related to the adsorption site for the complex of pyridine adsorbed onto heteronuclear clusters.[11] Considering that SERS enhancement can be determined by both EM and CT mechanisms, there is a need to include the EM mechanism in the calculation, as it also plays a dominant role in SERS enhancements. In this study we adopted a recently developed TDDFT method which can simulate both IE and CT enhancement, and conducted a comprehensive study of the SERS enhancement based on the composition-tunability mechanism. The new approach uses a short-time approximation for the Raman cross-section calculation.

We obtained the absorption and SERS properties of MAg-Py (M=Cu, Ag, Au) complexes. The results indicate that the resonant excitation wavelengths, together with the characteristics and effect of SERS, depend strongly on the composition of metal clusters. Although the enhancements of the SERS at 489 nm (CuAg-Py) and at 470 nm (AuAg-Py) are weaker than that at 375 nm ($Ag_2$-Py), the excitations of the former two are close to the 488 nm laser and thus are more feasible for SERS detection. Thus, the heteronuclear metal clusters have advantages in tuning the excitation light in SERS experiments. Molecular orbital analysis results reveal that IE enhancement is not exclusive to the presence of CT enhancement. However, it is very interesting that for the SERS at 489 nm of the CuAg-Py complex, the Cu atom acts as donor to provide transitional charge in the process of excitation, as does the Au atom in the AuAg-Py complex in the process of SERS (369 nm) excitation, presenting a unique feature of heteronuclear metal clusters as SERS substrates, owing to the polarization between atoms of different metals.

Although the pyridine is adsorbed onto the silver atoms in all these three complexes, binding properties analysis indicates that the complexes of heteronuclear clusters are more stable than homonuclear clusters. The chemical and physical properties of complexes can also be tuned by varying the composition of metal clusters. Superior performances of mixed-metal materials are needed for the development of nanoscience and technology, and our study is expected to provide a theoretical basis for exploring novel multi-composition SERS materials that can be widely used in many fields, including characterization of nanostructures, SM-SERS detections, and biological molecular recognitions.

## Acknowledgements

The work described in this paper is supported by grants from the National Science Foundation of China under grant nos. 11374004 and 30870533, and the Research Grants Council of Hong Kong SAR [project no. CityU 103812]. Z. W. acknowledges the Fok Ying Tung Education Foundation (142001) and High Performance Computing Center (HPCC) of Jilin University.The main text of the article should go here with headings as appropriate.

## Notes and references

[a] *Key Laboratory for Molecular Enzymology and Engineering of Ministry of Education, College of Life Sciences, Jilin University, Changchun, 130012, China*
[b] *Institute of Atomic and Molecular Physics, Jilin University, Changchun 130012, China*
[c] *State Key Laboratory of Theoretical and Computational Chemistry, Jilin University, Changchun 130012, China*
[d] *Department of Physics and Materials Science and Centre for Functional Photonics (CFP), City University of Hong Kong, Hong Kong SAR, China*
[e] *Beijing Computational Science Research Center, Beijing 100084, P. R. China*
*wangzg@jlu.edu.cn; lzq@jlu.edu.cn; aprqz@cityu.edu.hk*

† Electronic Supplementary Information (ESI) available: [details of any supplementary information available should be included here]. See DOI: 10.1039/b000000x/

1 (a) M. Fleischmann, P. J. Hendra and A. J. McQuillan, *Chem. Phys. Lett.*, 1974, **26**, 163-166; (b) M. G. Albrecht and J. A. Creighton, *J. Am. Chem. Soc.*, 1977, **99**, 5215-5217.

2 (a) B. Paramanik and A. Patra, *J. Mater. Chem. C*, **2014**, 2, 3005-3012; (b) O. A. Roberto, R. Dmitrij, M. Philip A., P. Paul, M. Eric, A. G. Alán, *J. Phys. Chem. C*, 2012, **116**, 15568-15575.

3 (a) Y. Wang, L. Chen and P. Liu, *Chem. Eur. J*, 2012, **18**, 5935-5943; (b) K. Sun, G. Meng, Q. Huang, X. Zhao, C. Zhu, Z. Huang, Y. Qian, X. Wang and X. Hu, *J. Mater. Chem. C*, **2013**, 1, 5015-5022; (c) Y. Zhou, C. Lee, J. Zhang and P. Zhang, *J. Mater. Chem. C*, 2013, 1, 3695-3699; (d) Y. Yin, T. Qiu, L. B. Ma, X. Z. Lang, Y. Zhang, G. S. Huang, Y. F. Mei and O. G. Schmidt, *J. Phys. Chem. C*, 2012, **116**, 25504-25508.

4 P. P. Patra and G. V. P. Kumar, *J. Phys. Chem. Lett.*, 2013, **4**, 1167-1171.

5 A. Sivanesan, E. Witkowska, W. Adamkiewicz, L. Dziewit, A. Kaminska and J. Waluk, *Analyst*, 2013, **139**, 1037-1043.

6 S. M. Morton, D. W. Silverstein and L. Jensen, *Chem.Rev.*, 2011, **111**, 3962-3994.

7 R. Aroca and S. Rodriguez-Llorente, *J.Mol. Struct.*, 1997, 408–409, 17-22.

8 K. Kneipp, H. Kneipp and J. Kneipp, *Acc. Chem. Res.*, 2006, **39**, 443-450.

9 B. N. J. Persson, K. Zhao and Z. Y. Zhang, *Phys. Rev. Lett.*, 2006, **96**, 207401.

10 (a) M. Fan, F. J. Lai, H. L. Chou, W. T. Lu, B. J. Hwang and A. G. Brolo, *Chem. Sci.*, 2013, **4**, 509-515; (b) J. Suntivich, Z. C. Xu, C.



 

E. Carlton, J. Kim, B. H. Han, S. W. Lee, N. Bonnet, N. Marzari, L. F. Allard, H. A. Gasteiger, K. Hamad-Schifferli and Y. Shao-Horn, *J. Am. Chem. Soc.*, 2013, **135**, 7985-7991; (c) N. E. Motl, E. Ewusi-Annan, I. T. Sines, L. Jensen and R. E. Schaak, *J. Phys. Chem. C*, 2010, **114**, 19263-19269.

11 L. Chen, Z. Q. Li, Y. Meng, M. Lu, Z. Wang and R. Q. Zhang, *J. Phys. Chem. C*, 2013, **117**, 12544-12551.

12 D. Y. Wu, B. Ren and Z. Q. Tian, *Chemphyschem*, 2006, **7**, 619-628.

13 (a) S. Wei, Q. Wang, J. Zhu, L. Sun, H. Lin and Z. Guo, *Nanoscale*, 2011, **3**, 4474-4502; (b) X. L. Tang and M. Tsuji, *CrystEngComm*, 2011, **13**, 72.

14 H. Xu, J. Aizpurua, M. Kall and P. Apell, *Phys. Rev. E.*, 2000, **62**, 4318-4324.

15 E. C. Le Ru and P. G. Etchegoin, *Annu. Rev. Phys. Chem.*, 2012, **63**, 65-87.

16 S. Habuchi, M. Cotlet, R. Gronheid, G. Dirix, J. Michiels, J. Vanderleyden, F. C. De Schryver and J. Hofkens, *J. Am. Chem. Soc.*, 2003, **125**, 8446-8447.

17 S. Nie and S. R. Emory, *Science*, 1997, **275**, 1102-1106.

18 K. Kneipp, Y. Wang, H. Kneipp, L. T. Perelman, I. Itzkan, R. R. Dasari and M. S. Feld, *Phys. Rev. Lett.*, 1997, **78**, 1667-1670.

19 H. Xu, E. J. Bjerneld, M. Käll and L. Börjesson, *Phys. Rev. Lett.*, 1999, **83**, 4357-4360.

20 (a) D. Y. Wu, M. Hayashi, C. H. Chang, K. K. Liang and S. H. Lin, *J. Chem. Phys.*, 2003, **118**, 4073; (b) D. Y. Wu, M. Hayashi, S. H. Lin and Z. Q. Tian, *Spectrochi. Acta. A*, 2004, **60**, 137-146.

21 L. L. Zhao, L. Jensen and G. C. Schatz, *J. Am. Chem. Soc.*, 2006, **128**, 2911-2919.

22 L. Jensen, C. M. Aikens and G. C. Schatz, *Chem. Soc. Rev.*, 2008, **37**, 1061-1073.

23 C. M. Aikens and G. C. Schatz, *J. Phys. Chem. A*, 2006, **110**, 13317-13324.

24 D. Masiello and G. C. Schatz, *J. Chem. Phys.*, 2010, **132**, 064102.

25 D. Y. Wu, X. M. Liu, S. Duan, X. Xu, B. Ren, S. H. Lin and Z. Q. Tian, *J. Phys. Chem. C*, 2008, **112**, 4195-4204.

26 (a) L. Jensen, J. Autschbach and G. C. Schatz, *J. Chem. Phys.*, 2005, **122**, 224115; (b) L. Jensen, L. L. Zhao, J. Autschbach and G. C. Schatz, *J. Chem. Phys.*, 2005, **123**, 174110.

27 R. L. Birke, V. Znamenskiy and J. R. Lombardi, *J. Chem. Phys.*, 2010, **132**, 214707.

28 (a) G. A. Bishea, N. Marak and M. D. Morse, *J. Chem. Phys.*, 1991, **95**, 5618-5629; (b) G. A. Bishea and M. D. Morse, *J. Chem. Phys.*, 1991, **95**, 5646-5659; (c) V. Beutel, H.G. Krämer, G. L. Bhale, M. Kuhn, K. Weyers, and W. Demtröder, *J. Chem. Phys.*, 1993, **98**, 2699-2708; (d) C. Felix, C. Sieber, W. Harbich, J. Buttet, I. Rabin, W. Schulze, G. Ertl, *Chem. Phys. Lett.*, 1999, **313**, 105-109; (e) V. Kellö and A. J. Sadlej, *J. Chem. Phys.*, 1995, **103**, 2991; (f) S. Fedrigo, W. Harbich and J. Buttet, *Phys. Rev. B*, 1993, **47**, 10706-10715.

29 M. Sun, S. Wan, Y. Liu, Y. Jia and H. Xu, *J. Raman Spectrosc.*, 2008, **39**, 402-408.

30 (a) G. te Velde, F. M. Bickelhaupt, E. J. Baerends, C. Fonseca Guerra, S. J. A. van Gisbergen, J. G. Snijders and T. Ziegler, *J. Comput. Chem.*, 2001, **22**, 931-967; (b) D. V. Chulhai and L. Jensen, *J. Phys. Chem. C*, 2013, **117**, 19622-19631.

31 (a) A. D. Becke, *Phys. Rev. A*, 1988, **38**, 3098-3100; (b) J. P. Perdew, *Phys. Rev. B*, 1986, **33**, 8822-8824.

32 L. Jensen, L. L. Zhao and G. C. Schatz, *J. Phys. Chem. C*, 2007, **111**, 4756-4764.

33 S. M. Morton and L. Jensen, *J. Am. Chem. Soc.*, 2009, **131**, 4090-4098.

34 (a) E. van Lenthe, E. J. Baerends and J. G. Snijders, *J. Chem. Phys.*, 1993, **99**, 4597-4610; (b) E. van Lenthe, E. J. Baerends and J. G. Snijders, *J. Chem. Phys.*, 1994, **101**, 9783-9792.

35 J. Neugebauer and B. A. Hess, *J. Chem. Phys.*, 2003, **118**, 7215-7225.

36 J. Neugebauer, M. Reiher, C. Kind and B. A. Hess, *J. Comput. Chem.*, 2002, **23**, 895-910.

37 A. Vivoni, R. L. Birke, R. Foucault and J. R. Lombardi, *J. Phys. Chem. B*, 2003, **107**, 5547-5557.

PCCP RSCPublishing

ARTICLE

Table of Contents

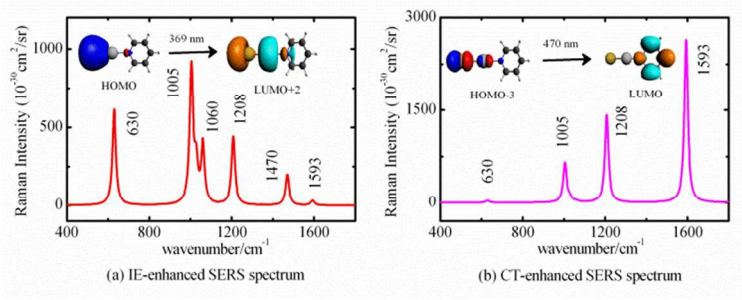


SERS spectra of the AuAg-Py complex: (a) an IE-enhanced spectrum at an incident wavelength of 369 nm, and (b) a CT-enhanced spectrum at an incident wavelength of 470 nm.